Micromixing effects on series–parallel and autocatalytic reactions in a turbulent single-phase gas flow

ARTICLE *in* CHEMICAL ENGINEERING SCIENCE · AUGUST 2010

Impact Factor: 2.34 · DOI: 10.1016/j.ces.2010.05.011

3 AUTHORS, INCLUDING:

S.N.P. Vegendla
Argonne National Laboratory
22 PUBLICATIONS **63** CITATIONS

SEE PROFILE

Geraldine J. Heynderickx
Ghent University
94 PUBLICATIONS **974** CITATIONS

SEE PROFILE

Chemical Engineering Science 65 (2010) 4621–4629

Contents lists available at ScienceDirect

Chemical Engineering Science

journal homepage: www.elsevier.com/locate/ces

Micromixing effects on series–parallel and autocatalytic reactions in a turbulent single-phase gas flow

S.N.P. Vegendla, G.J. Heynderickx *, G.B. Marin

Universiteit Gent, Laboratorium voor Chemische Technologie, Krijgslaan 281, S5, Gent 9000, Belgium

ARTICLE INFO

Article history:
Received 27 January 2010
Received in revised form
22 April 2010
Accepted 8 May 2010
Available online 31 May 2010

Keywords:
Micromixing
Stochastic differential equation (SDE)
Interaction-by-exchange-with-the-mean (IEM)
Autocatalytic reactions
Series–parallel reactions
Probability density function (PDF)

ABSTRACT

A hybrid solution algorithm is implemented to simulate turbulent reactive single-phase gas flow in an isothermal tubular reactor. This algorithm is a combination of a Finite Volume (FV) and a Probability Density Function (PDF) method. The FV method is used to solve the mass and momentum conservation equations combined with a standardized k–ε model for single-phase gas flow. The PDF method is applied to solve the species continuity equations. The advantage of using the PDF method is the fact that there is no need of any closures for chemical reaction source terms in a turbulent flow. The mesomixing and the micromixing contributions in the PDF equation are closed using the gradient-diffusion model and the Interaction-by-Exchange-with-the-Mean (IEM) model, respectively. This hybrid solution algorithm is applied to simulate a series–parallel and an autocatalytic reactive single-phase gas flow. The mechanical-to-scalar time-scale ratio, i.e. the IEM model parameter, is found to have an influence on the simulation results that cannot be neglected. As expected, in series–parallel reactions, the desired product selectivity increases when the reaction rate coefficient, corresponding to its formation, increases. Moreover multiple solutions are observed in the autocatalytic reaction for a given feed ratio, Damköhler (Da^I) and Péclet (Pe) numbers. To validate the hybrid FV–PDF solution algorithm, the calculated results are compared with the results obtained when using the Reynolds-averaged species continuity equation model. A good agreement is observed when infinite-rate mixing is applied.

1. Introduction

Chemical reactor design is a major area of research from an industrial point of view. The design is relatively simple for a laminar flow reactor, but becomes more difficult for turbulent flow reactors. Nevertheless, the majority of chemical reactors operate in the turbulent flow regime. Turbulent flow makes the control of the reactor temperature easier. Turbulent flow is preferred as heat and mass transfer rates are high as compared to laminar flow reactors, at least at a typical industrial scale. Turbulent flow is also required to obtain higher throughputs, which makes the turbulent flow reactor more interesting from an economical point of view (Vassilatos and Toor, 1965).

When a chemical reaction takes place in a turbulent fluid, the local instantaneous rate of reaction, i.e. the rate of the reaction equal to the mean reaction rate plus the rate of the reaction due to fluctuations, is assumed to follow the basic laws of chemical kinetics. The mean reaction rate r_i, i.e. the time-averaged or ensemble-averaged, may be higher than, equal to, or lower than the instantaneous reaction rate. The above statement is true, whether the system is isothermal or not. In a homogeneous mixture, i.e. when the root mean square (RMS) concentration fluctuations of all species can be neglected, the mean reaction rate equals the instantaneous reaction rate. The latter statement is valid even in a non-homogeneous mixture, if the reaction is of first order.

Reactions can be classified as follows: (i) very rapid reactions, i.e. mixing controlled; (ii) rapid reactions, i.e. both mixing and kinetically controlled; and (iii) slow reactions, i.e. kinetically controlled (Vassilatos and Toor, 1965; Mao and Toor, 1970; Hebb and Brodkey, 1990). This corresponds, respectively, to situations, where the reaction rate is potentially much faster than the mixing rate, the reaction rate is of the same order as the mixing rate, and the reaction rate is much slower than the mixing rate.

One of the critical issues in modeling a turbulent reactive flow is the interaction between the chemical reaction and the turbulent mixing process. Accurate modeling and simulation of turbulent reactive flows is still not fully developed. This is mainly due to the complexity of correctly describing the coupling between fluid dynamics and chemistry at the microscale level.

In turbulent reactive flows, guidelines are needed to choose direct closure techniques in conventional models such as

* Corresponding author. Tel.: +32 0 92644532; fax: +32 0 92644999.
E-mail address: Geraldine.Heynderickx@UGent.be (G.J. Heynderickx).

0009-2509/$ - see front matter © 2010 Elsevier Ltd. All rights reserved.
doi:10.1016/j.ces.2010.05.011

Reynolds-averaged Navier–Stokes (RANS) (Vassilatos and Toor, 1965) and large-Eddy simulations (LES) (Fox, 2003). These closure techniques are a function of kinetics of the reaction, the diffusion of the species in the reactor, the turbulent flow, the mean species concentration and their variance. Depending on the complexity of the approach, information on higher order moments, cross moments and multipoint moments of species can be obtained in the simulations (Fox, 2003). Applying reasonable hypotheses can make it possible to relate unknown terms in the set of conservation equations that describe the problem to the mean concentration of the reacting components and the turbulent field characteristics (Toor, 1969). These so-called closures can be further used for modeling and design purposes.

Series–parallel reactions, such as chlorination, halogenations or nitration of hydrocarbons are common in industrial processes. For all the above mentioned processes, the selectivity towards the desired product is highly dependent on the mixing of the reactants/products. The paper of Bourne et al. (1981) was the first in a series of publications, where the Bourne's reaction system (series–parallel reaction), was used in a Continuously stirred tank reactor (CSTR). Brodkey and Lewalle (1985), Li and Toor (1986), Mehta and Tarbell (1987) and Vrieling and Nieuwstadt (2003) also studied this reaction type in a tubular reactor. Brodkey and Lewalle (1985) performed numerical simulations for this reaction type using an extended Toor's hypothesis as a reaction closure in turbulent flow (Toor, 1969). In a next step, the bulk-averaged model was proposed by Vrieling and Nieuwstadt (2003). The latter model is referred to as the low-dimensional model.

Examples of single-phase autocatalytic reactions include the decomposition of $C_2H_4I_2$, either in the gas phase or in a CCl_4 solution, hydrolysis of an ester, and some microbial fermentation reactions (Missen et al., 1999). For a laminar flow, Gupta and Chakraborty (2009) performed autocatalytic reactive simulations using three different models of varying dimensionality. The 3D convection–diffusion–reaction (CDR) model is the high-dimensional model, while the Liapunov–Schmidt reduction based spatially averaged two-dimensional CDR model and its regularized form are the two low-dimensional ones. More details can be found in Chakraborty and Balakotaiah (2002, 2003); Balakotaiah and Chakraborty (2003) and Pushpavanam (2004). Yablonsky et al. (2009) performed a so-called reactive mixing index (REMI) analysis, to study the ideal and non-ideal reactor performance by using a small perturbation of one of the reactant concentrations at the reactor inlet.

The advantage of the PDF method is the exact treatment of the reaction source terms in the species continuity equations, without the need for any reaction closures. Merits and demerits are discussed in Pope (1985) and Fox (2003). Raman et al. (2004) and Kolhapure et al. (2005) have implemented PDF methods and promising results have been obtained for single-phase gas flow. Formulation of the PDF methods and solution procedures are discussed in detail in their work. Tsai and Fox (1996) implemented the PDF method for a series–parallel reaction in a single-jet tubular reactor, i.e. for a non-premixed feed.

In the present work, uniform feed concentrations, i.e. a premixed feed, are considered. The turbulence in a specific reactor, the mixing and its dependency upon the turbulent field, and the relation between mixing and chemical reactions is studied in an isothermal tubular reactor with (1) series–parallel reactions and (2) autocatalytic reactions.

Whereas the applied mathematical modeling is presented in Section 2, the solution procedure for a PDF method is demonstrated in Section 3. The hybrid solution algorithm for a single-phase reactive gas flow and the results obtained using the PDF method is dealt with in Sections 4 and 5, respectively. The major findings are summarized in the Section 6.

2. Mathematical modeling

Modeling of a reactive single-phase gas flow consists of two blocks: (1) modeling the flow and (2) modeling the reactions. The set of flow equations to be solved are the total mass, momentum and k–ε turbulence equations. As the reactor is assumed to be isothermal, the energy equation is not considered. These equations are well-known as the RANS equations.

2.1. Flow equations

2.1.1. Continuity equation

$$\frac{\partial}{\partial t}(\rho)+\frac{\partial}{\partial \mathbf{y}}.(\rho\overline{\mathbf{u}})=0 \tag{1}$$

2.1.2. Momentum equations (x, y, z)

$$\frac{\partial}{\partial t}(\rho\overline{\mathbf{u}})+\frac{\partial}{\partial \mathbf{y}}.(\rho\overline{\mathbf{u}}\,\overline{\mathbf{u}})=-\frac{\partial(\overline{P}+(2/3)\rho k)\delta_{ij}}{\partial \mathbf{y}}-\frac{\partial}{\partial \mathbf{y}}.(\overline{s})+\rho\mathbf{g} \tag{2}$$

where

$$\overline{s}=\overline{s^m}+s_{ij}^t=-\left[\left(\xi-\frac{2}{3}\mu\right)\left(\partial.\frac{\overline{\mathbf{u}}}{\partial \mathbf{y}}\right)+(\mu+\mu^t)\left\{\left(\partial\frac{\overline{\mathbf{u}}}{\partial \mathbf{y}}\right)+\left(\partial\frac{\overline{\mathbf{u}}}{\partial \mathbf{y}}\right)^T\right\}\right]$$

2.1.3. Turbulent kinetic energy equation

$$\frac{\partial}{\partial t}(\rho k)+\frac{\partial}{\partial \mathbf{y}}\cdot(\rho\overline{\mathbf{u}}k)=\frac{\partial}{\partial \mathbf{y}}\cdot\left(\frac{\mu+\mu^t}{\sigma_k}\frac{\partial k}{\partial \mathbf{y}}\right)+\left[\mu^t\left[\left(\partial\frac{\overline{\mathbf{u}}}{\partial \mathbf{y}}\right)+\left(\partial\frac{\overline{\mathbf{u}}}{\partial \mathbf{y}}\right)^T\right]\right]:\left(\partial\frac{\overline{\mathbf{u}}}{\partial \mathbf{y}}\right)-\rho\varepsilon \tag{3}$$

2.1.4. Turbulence kinetic energy dissipation equation

$$\frac{\partial}{\partial \mathbf{y}}(\rho\varepsilon)+\frac{\partial}{\partial \mathbf{y}}\cdot(\rho\overline{\mathbf{u}}\boldsymbol{\varepsilon})=\frac{\partial}{\partial \mathbf{y}}\cdot\left(\frac{\mu+\mu^t}{\sigma_\varepsilon}\frac{\partial\varepsilon}{\partial \mathbf{y}}\right)+C_{1\varepsilon}\frac{\varepsilon}{k}\left[\mu^t\left[\left(\frac{\partial}{\partial \mathbf{y}}\overline{\mathbf{u}}\right)+\left(\frac{\partial}{\partial \mathbf{y}}\overline{\mathbf{u}}\right)^T\right]:\left(\frac{\partial}{\partial \mathbf{y}}\overline{\mathbf{u}}\right)\right]-C_{2\varepsilon}\rho\frac{\varepsilon^2}{k} \tag{4}$$

where

$$\mu^t=C_\mu\rho\frac{k^2}{\varepsilon} \tag{5}$$

2.2. Reaction equations

For the species continuity equation, two methods are presented: (1) conventional method based on the Reynolds averaging approach and (2) the Probability Density Function (PDF) method.

2.2.1. Reynolds-averaged species continuity equation

The time-averaged instantaneous species continuity equation is defined as (Bird et al., 2002)

$$\frac{\partial(\overline{C}_i)}{\partial t}+\frac{\overline{\mathbf{u}}\partial(\overline{C}_i)}{\partial \mathbf{y}}=-\left(\frac{\mu^t}{\rho}+D_i\right)\frac{\partial}{\partial \mathbf{y}}\left[\nabla^2\overline{C}_i\right]-R(\overline{C}_i+C_i^t) \tag{6}$$

The first term on the left hand side (LHS) of this equation is the rate of change of the species concentration, the second term represents convection.

The first term on the right hand side (RHS) of this equation represents the diffusivity and the second term represents the reaction source term and its fluctuations.

Two contributions to Eq. (6) need to be closed, on the one hand the first term on the RHS for a turbulent viscosity of gas (μ^t), which is closed by using Eq. (5). On the other hand, the second term on the RHS for fluctuations in the rate of reaction ($R(Ct^i)$). The latter term is assumed to be negligible if the species are mixed well, i.e. the time scale of reaction is higher than the time scale of mixing.

Solving Eq. (6) is similar to solving the flow equations using the FV technique. More details on how to solve the Reynolds-averaged species continuity equations can be found in Das et al. (2004).

2.2.2. Transported composition PDF

The PDF $f_{\boldsymbol{\varphi}}(\boldsymbol{\Psi};\ y, t)$ is defined as the probability of observing the event that the values of the composition $\boldsymbol{\varphi}$ at a time t and a position y are found in the differential neighborhood of given values $\boldsymbol{\Psi}$

$$f_{\boldsymbol{\varphi}}(\boldsymbol{\Psi};\ y, t)d\boldsymbol{\psi} = P(\boldsymbol{\Psi} < \boldsymbol{\varphi} \le \boldsymbol{\Psi} + d\boldsymbol{\Psi}) \tag{7}$$

The one-point transported composition PDF equation is defined as (Kolhapure et al., 2005)

$$\frac{\partial(f_{\boldsymbol{\varphi}})}{\partial t} + \frac{\overline{\mathbf{u}}\partial(f_{\boldsymbol{\varphi}})}{\partial \mathbf{y}} + \frac{\partial}{\partial \mathbf{y}}\left[\langle u_i' | \boldsymbol{\Psi}\rangle f_{\boldsymbol{\varphi}}\right] = -\frac{\partial}{\partial \psi_\alpha}\left[\langle D_\alpha \nabla^2 \varphi_\alpha | \boldsymbol{\Psi}\rangle f_{\boldsymbol{\varphi}}\right] - \frac{\partial}{\partial \psi_\alpha}\left[R_\alpha(\boldsymbol{\Psi}) f_{\boldsymbol{\varphi}}\right] \tag{8}$$

where $< >$ represents the ensemble average, based on a specified number of samples.

The first term on the left hand side (LHS) of this equation is the rate of change of probability; the second term represents convection (macromixing); and the third term represents scalar-conditioned velocity fluctuations (mesomixing).

The first term on the right hand side (RHS) of this equation is the scalar-conditioned dissipation (micromixing) and the second term represents the reaction source term.

Two contributions to Eq. (8) need to be closed, one is the third term on the LHS (mesomixing) and the other one is the first term on the RHS (micromixing).

Mesomixing:

The scalar-conditioned velocity fluctuation contribution is closed using the gradient-diffusion model (Raman et al., 2004)

$$\langle \mathbf{u}' | \boldsymbol{\Psi}\rangle f_{\boldsymbol{\varphi}} = -\frac{\mu^t}{\rho Sc^t}\frac{\partial f_{\boldsymbol{\varphi}}}{\partial \mathbf{y}} = -D^t \frac{\partial f_{\boldsymbol{\varphi}}}{\partial \mathbf{y}} \tag{9}$$

Micromixing:

The scalar-conditioned dissipation is closed by the Interaction-by-Exchange-with-the-Mean (IEM) model, which assumes a linear relaxation of the scalar towards its mean value (Villermaux, 1986; Raman et al., 2004; Cassiani et al., 2005)

$$\langle D_\alpha \nabla^2 \boldsymbol{\varphi} | \boldsymbol{\Psi}\rangle = \frac{1}{\tau_\varphi}(\langle \boldsymbol{\varphi}(\mathbf{y}, t)\rangle - \boldsymbol{\Psi}_\alpha) \tag{10}$$

where $\langle \boldsymbol{\varphi}(\mathbf{y}, t)\rangle$ is the local scalar mean at position $\mathbf{y}$ and time t, and τ_ϕ is the local micromixing time calculated using a separate model for the scalar dissipation rate as described in Fox (2003)

$$C_\phi \tau_\phi \cong \frac{k}{\varepsilon} \cong \tau_u \tag{11}$$

where C_ϕ is the mechanical-to-scalar time-scale ratio, a constant that needs to be determined to describe the micromixing.

3. Solution procedure

Solving the one-point transported composition PDF equation (Eq. (8)), using standard solution methods such as the Finite Volume (FV) or the Finite Differences (FD) method is computationally prohibitive for a large number of species. Therefore, a Monte-Carlo particle-mesh technique is implemented (Vegendla et al., 2009). The one-point transported composition PDF equation is represented by a large number of so-called notional particles, randomly and continuously distributed over the flow domain (Fox, 2003). The transported composition PDF is solved for a sufficiently large number of notional particles in order to obtain an accurate estimate of the mean composition field.

$$\langle \boldsymbol{\varphi}_l \rangle = \frac{\sum_{n=1}^{N_l} m_l^n \boldsymbol{\varphi}_l^n}{\sum_{n=1}^{N_l} m_l^n} \tag{12}$$

where m_l^n is the mass of the notional particle and $\boldsymbol{\varphi}_l^n$ is the chemical composition vector for the nth particle in a given mesh cell 'l'.

The position of these notional particles in physical space (Eq. (13)) and their corresponding composition (Eq. (14)) are determined by solving a set of stochastic differential equations (SDEs). The SDEs for the notional particles are the replicas of the transported composition PDF equation (Eq. (8)) (Raman et al., 2004).

The SDE to determine the position of the bulk gas phase notional particle (Eq. 13), for single-phase gas flow is given by (Kolhapure et al., 2005)

$$d\mathbf{y^n} = \left(\overline{\mathbf{u}} + \frac{\nabla(\mu+\mu^t)}{\langle \rho \rangle}\right)dt + \sqrt{2\frac{(\mu+\mu^t)}{\langle \rho \rangle}}d\boldsymbol{W} \tag{13}$$

where the first term on the RHS of Eq. (13) represents the convection arising from the mean velocity, the molecular and the turbulent diffusivity of the bulk gas phase. The second term on the RHS represents the Wiener-diffusion process ($d\boldsymbol{W}$), characterized by a Gaussian process with zero mean and variance dt (Kolhapure et al., 2005).

The SDE to determine the composition of a notional particle in the bulk gas phase (Eq. 14), for single-phase gas flow is given by (Kolhapure et al., 2005)

$$d\boldsymbol{\varphi}^n = \left(\frac{C_\varphi}{2\tau_\varphi}(\langle \boldsymbol{\varphi} \rangle - \boldsymbol{\varphi}^n) + R(\boldsymbol{\psi})\right)dt \tag{14}$$

The terms on the RHS of Eq. (14) represent the micromixing term (IEM) and the reaction source term in composition space.

3.1. Notional-particle tracking

The Monte-Carlo numerical solution technique for the transported composition PDF equations demands a Lagrangian–Eulerian approach. Each notional particle has to be associated with a grid cell in the computational domain. Lagrangian tracking of the notional particles is done in three steps: (1) determine the cell a notional particle is located in; (2) interpolate the field variables at the notional-particle location; and (3) update the position of the particle according to the velocity vector and the turbulent diffusivity within the gas phase (Eq. (13)), using a time integration method (see Section 3.3).

In the first step, the position of the notional particles is to be determined. Three possible algorithms are available: the brute-force algorithm, the modified brute-force algorithm, and the known-vicinity search algorithm, as reported by Apte et al. (2003).

In the present work, the modified brute-force algorithm is implemented. This algorithm determines the mesh point closest

to the notional-particle location, and considers the grid cells that surround this mesh point. The face-to-face strategy is implemented to find the notional-particle location. This strategy projects the notional-particle location onto the faces of the grid cell under consideration and compares the obtained vectors with the outward face-normals for all faces of the grid cell. If the particle is positioned within the grid cell, the projected vectors point in the same direction as the outward face-normals. This technique is found to be very accurate, even for highly skewed meshes (Subramaniam and Haworth, 2000; Apte et al., 2003).

In the second step, the flow variables must be interpolated to attain their values in the notional-particle location. In practice, the grids used in many CFD applications are not Cartesian. To handle complex reactor geometries like a riser reactor, curvilinear grids are used (De Wilde et al., 2003). Such grids are also referred to as structured grids, because they have a regular topological structure, as opposed to unstructured grids. The information on the gas properties obtained by solving the flow model equations using the FV technique is available at the centre of each grid cell. Several schemes can be used to interpolate these flow properties to the notional-particle location (Sadarjoen et al., 1997). A tri-linear interpolation scheme with an inverse distance weighing algorithm is implemented for the curvilinear grid used in the present work.

In the third and last step, the position of the notional particle is updated. Evaluating the position of the notional particle at each time step is described in Section 3.3.

3.2. Boundary conditions for notional-particle tracking

Boundary conditions (BC) must be applied at the edge of the physical simulation domain during the Monte-Carlo (MC) simulations. The four most common types of BC are inflow, outflow, symmetry and zero-flux wall BC. The procedure for inflow, outflow and zero-flux wall BC is implemented as explained by Fox (2003).

3.3. Time-stepping formulation for position and composition updates of the notional particle

For each time step, the transport and chemical reaction contributions to the time derivative term are calculated using two different operators for the geometrical space (Eq. (13)) and the composition space (Eq. (14)). The time-stepping formulation involves the following steps to update the solution of the SDEs for the nth notional-particle position and composition:

(1) The hydrodynamic properties, i.e. velocities, pressure, turbulent kinetic energy and turbulent kinetic energy dissipation, are used to initialize the notional particle by using a tri-linear interpolator, (Apte et al., 2003) at the beginning of the time step.

(2) The position of the nth notional particle is updated using the first-order accurate Euler Scheme (Kolhapure et al., 2005). The simplest numerical method to integrate the notional-particle position SDEs (Eq. (13)) is the explicit forward Euler scheme, in which the solution is advanced from time t_o to time $t_o+\Delta t$ as

$$\mathbf{y^n}(t_o+\Delta t)=\mathbf{y^n}(t_o)+(\langle \mathbf{u}\rangle(\mathbf{y}^n[t_o],\, t_o)+\Gamma_t(\mathbf{y}^n[t_o],\, t_o))\Delta t + \sqrt{2\Gamma_t(\mathbf{y}^n[t_o],\, t_o)}\Delta t^{1/2}\xi \quad (15)$$

where ξ is a standardized Gaussian random vector ($<\xi>=0$, and $<\xi_i\ \xi_j>=\delta_{ij}$). This method is only first-order accurate. The second term on the RHS of Eq. (15) corresponds with the first term on the RHS of Eq. (13), while the third term on the RHS of Eq. (15) corresponds with the second term on the RHS of Eq. (13). The Wiener-diffusion ($d\boldsymbol{W}$) process (Kolhapure et al., 2005) is included in the integration result via $\Delta t^{1/2}\xi$.

(3) Finally, the composition vector of the nth notional particle is updated using the fractional time-stepping procedure. The composition vector is first updated making a full time step for the transport term (i.e. the micromixing contribution) (Eq. (16)). Next, the reaction step is updated by using a Direct Integration (DI) method (Eq. (17)).

$$\boldsymbol{\varphi^{n*}}=\langle\boldsymbol{\varphi}\rangle+\exp\left(\frac{-C_\varphi\, dt}{2\tau_\varphi}\right)(\boldsymbol{\varphi^n}-\langle\boldsymbol{\varphi}\rangle) \quad (16)$$

$$\boldsymbol{\varphi^n}=\boldsymbol{\varphi^{n*}}+\int_t^{t+\Delta t} R(\psi)\, dt \quad (17)$$

4. Hybrid algorithm

As seen in Fig. 1, the flow and reaction equations are solved separately by using a decoupled solver (Vegendla et al., 2009) for single-phase gas flow. In the present work, density variations are considered to be negligible, i.e. the reactions will not affect the flow of the gas. The FV method is used to solve the flow equations. An extensive discussion of the solution procedure is found in De Wilde et al. (2003) and Das et al. (2004). The transported composition PDF equations for reactive species, however, are solved by using the notional-particle approach as described above. In this work, flow simulations are performed until the specified flow convergence criteria are met. Next, the set of SDEs are solved to obtain the corresponding species concentrations.

5. Results and discussion

Three dimensional simulations of series–parallel and auto-catalytic reactions are performed in an isothermal tubular reactor

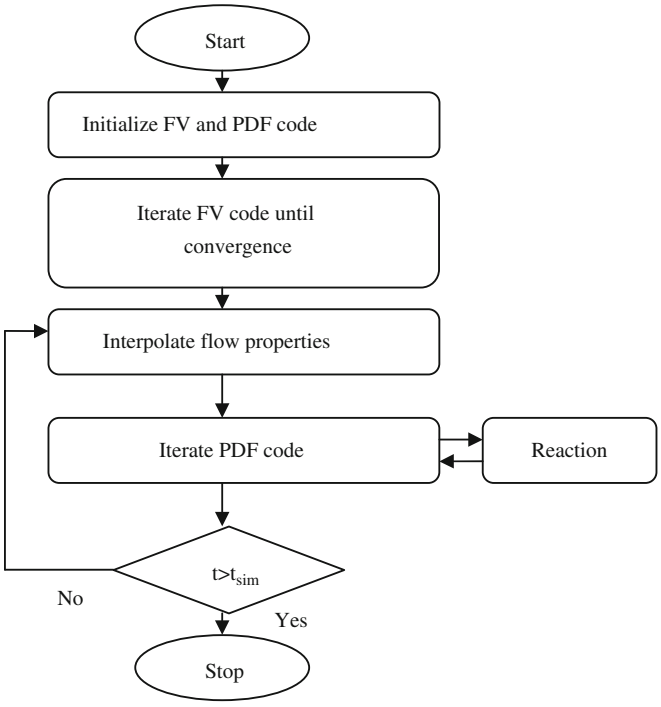

Fig. 1. Simulation procedure for reactive riser flow.

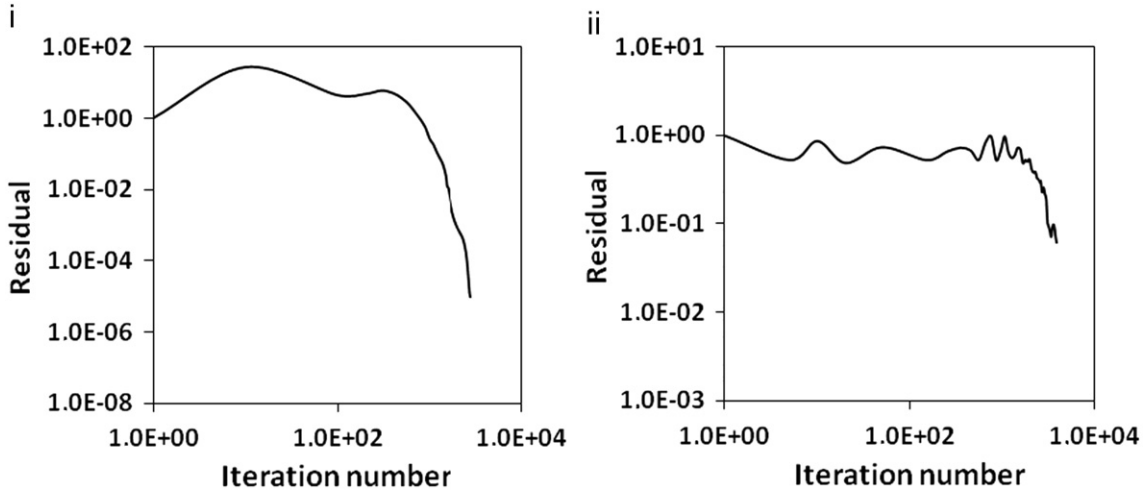

Fig. 2. Log–log plot of normalized residuals vs. iteration number for (i) flow and (ii) autocatalytic reaction ($u=3$ m s^{-1}, $C_\varphi=2$, $\beta=1$ and $\gamma=0.02$).

with a tube length of 4.5 cm and a diameter of 0.5 cm. An average inlet velocity 3 m/s is considered as an operating condition for the series–parallel reactive simulation. Average inlet velocities of 1, 3 and 6 m/s are considered for the autocatalytic reactive simulations. The present results are obtained in the reactor geometry using a total number of 965 cells with 100 notional particles for each cell. As seen in Fig. 2, to meet the required convergence criteria, the residuals are set to drop around six orders of magnitude for flow and two orders of magnitude for reaction. The total amount of CPU time for flow is around 48 h and the total amount of CPU time for reaction for each run of the specified parameters, i.e. micromixing and reaction rate constants, is around 4 h on a Xeon processor having 1.4 GHz and 1 GB RAM on a linux operating system 9.0. Time averaging is performed in a PDF code to reduce the statistical errors, after reaching a statistically stationary state by using $<\varphi^{i+1}>=(1-N_{TA}^{-1})<\varphi^{i}>+N_{TA}^{-1}<\varphi^{i+1}>$, (a N_{TA} of 3000 is used).

The obtained results are validated based on available literature data (Brodkey and Lewalle, 1985; Gupta and Chakraborty, 2009) for different mechanical-to-scalar time-scale values C_Φ (see Eq. (11)).

5.1. Series–parallel reactions

Series–parallel reactions (Bourne and Toor, 1977; Bourne et al., 1981) with varying reaction rate coefficients and IEM mixing model parameters C_Φ have been implemented.

$$A+B\rightarrow P \tag{18}$$

$$P+B\rightarrow S \tag{19}$$

$$R_A=-k_1C_AC_B \tag{20}$$

$$R_B=-k_1C_AC_B-k_2C_PC_B \tag{21}$$

$$R_P=k_1C_AC_B-k_2C_PC_B \tag{22}$$

$$R_S=k_2C_PC_B \tag{23}$$

The initial conditions for the simulations are $C_{Bo}/C_{Ao}=\gamma$, $C_{Po}=0$, $C_{So}=0$, where γ is the feed ratio. A normalized concentration C_i^* of the different components is defined as: $C_A^*=C_A/C_{Ao}$, $C_B^*=C_B/(\gamma C_{Ao})$, $C_P^*=C_P/C_{Ao}$, $C_S^*=C_S/C_{Ao}$.

Brodkey and Lewalle (1985) introduced ad-hoc models as closure models for the reaction source terms in the time-averaged species continuity equations for a combination of series–parallel reactions, considering the mixing effects in the reactor. The advantage of using the present transported composition PDF method is the fact that there is no need for closure of these reaction source terms in a turbulent reactive flow, as already discussed in the introduction.

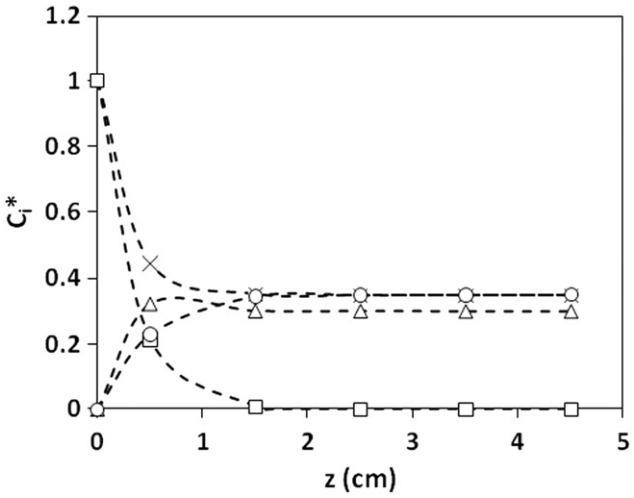

Fig. 3. Normalized concentrations C_i^* vs. tube length, (symbols: x—C_A^*; □—C_B^*; △—C_P^* and ○—C_S^* values are obtained by using the PDF approach (see Eq. (14)) and broken lines are obtained by using the Reynolds-averaged species continuity equations (see Eq. (6))), using complete mixing at sub-grid scale. Reaction rate coefficients $k_1=k_2=200$ m^3 mol^{-1} s^{-1}, feed ratio $\gamma=1$ and Rt$=0.8$.

As seen in Fig. 3, the comparison of normalized concentrations along the length of reactor by using the transported composition PDF method and the Reynolds-averaged species continuity equations (see Eq. (6)) solved by using the FV technique are presented for an infinite-rate mixing. Similar results are observed for both the above mentioned methods, qualitatively as well as quantitatively. It also justifies to study the importance of the micromixing effects on the rate of reaction by using the transported composition PDF method. The hybrid FV/PDF method results are presented in the following paragraphs.

As seen in Fig. 4, the selectivity, defined as the ratio of C_P/C_S, decreases with increasing mixing intensity I. The mixing intensity is defined as $1/\tau_\Phi$. As expected, the concentration of the

component S in the mixture will rise with the well-mixedness of the reactor, i.e. with increasing C_Φ. The same observation was made by Brodkey and Lewalle (1985).

As seen in Fig. 5, the formation of the component S in the reactor is high when using an infinite-rate mixing model (high value of C_Φ) (Fig. 5(ii)) as compared to the formation of the component S when the finite-rate mixing model is used (low value of C_Φ) (Fig. 5(i)). On the other hand, the conversion of A decreases when using the infinite-rate mixing model as compared to the finite-rate mixing model. This is due to the rising formation of *S* from the available P and B. The latter components are better mixed when using an infinite-rate mixing model, giving rise to a higher contribution of the reaction of these two components (Eq. (19)). Fig. 5 illustrates that the normalized concentrations of *A* and *S* are equal along the axial length of the reactor starting from 2.5 cm on. This is due to the fact that the reaction rate coefficients of k_1 and k_2 are equal for both reactions (Eqs. (18) and (19)). If these reaction rates are different (or the feed ratio γ changes), a clear difference in the normalized concentrations of *A* and *S* along the total axial length of the reactor (see Fig. 1 of Brodkey and Lewalle (1985)) will be calculated. As shown in Figs. 6 and 7 from Brodkey and Lewalle (1985), the selectivity C_P/C_S is highly dependent upon the reactor type (i.e. complete segregation reactor (CSR) to maximum mixedness reactor (MMR)) and upon the reaction rates. Note that Rt is the time ratio of a CSR to a non-ideal CSR. Brodkey and Lewalle (1985) have presented the results for different values of Rt (0.9, 0.3 and 0.1) with a mixing intensity *I* varying from 0 to $10^3\ s^{-1}$, and for reaction rate coefficients k_1 and k_2 varying from 200 to $10^4\ m^3\ mol^{-1}\ s$. The results presented in the work of Brodkey and Lewalle (1985) correspond to the present results. The results presented here are obtained over a broad range of the mixing intensity *I* from 0 to $10^4\ s^{-1}$, using identical values of the reaction rate coefficients k_1 and k_2, as Brodkey and Lewalle (1985) used, but with Rt equal to 0.8.

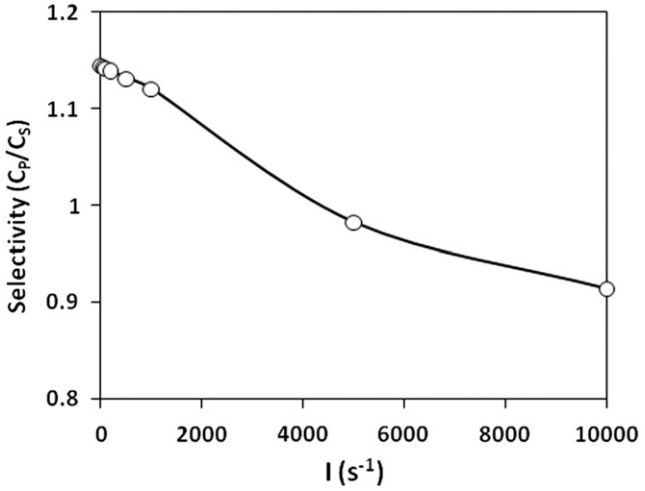

Fig. 4. Selectivity vs. mixing intensity with using reaction rate coefficients $k_1=k_2=10^4\ m^3\ mol^{-1}\ s^{-1}$, feed ratio $\gamma=1$ and Rt=0.8. The calculated selectivity is obtained from Eqs. (12) and (14).

As seen in Fig. 6(i), the rise of the selectivity with high and low, but equal, rising reaction rate coefficients k_1 and k_2 is observed for the same feeding condition ($\gamma=1$). The influence of using different reaction rate coefficient values for k_1 and k_2 is presented in Fig. 6(ii). A rise of selectivity is observed for a ratio of the reaction rate coefficients $k_1/k_2=3$ as compared to a ratio of 1 (see Fig. 6(i)). This is due to fact that if the reaction rate coefficient k_1 is high (Eq. (18)) as compared to the reaction rate coefficient k_2 (Eq. (19)), the formation of P is high. Bourne et al. (1981), made the same observation for well-mixed conditions. On the other hand, the selectivity drops (not shown) when using a reaction rate coefficients ratio of $k_1/k_2<1$. Finally, it can be concluded from Figs. 4 and 5 that, as expected, the selectivity of the series–parallel reactions highly depends on the mixing intensity *I* of the reaction mixture.

5.2. Autocatalytic reactions

The effect of different feeding ratios γ and of different IEM model parameter values C_Φ on the following autocatalytic reaction is investigated in a turbulent tubular reactive flow.

$$A+2B\rightarrow 3B \tag{24}$$

$$-R_A=R_B=kC_AC_B^2 \tag{25}$$

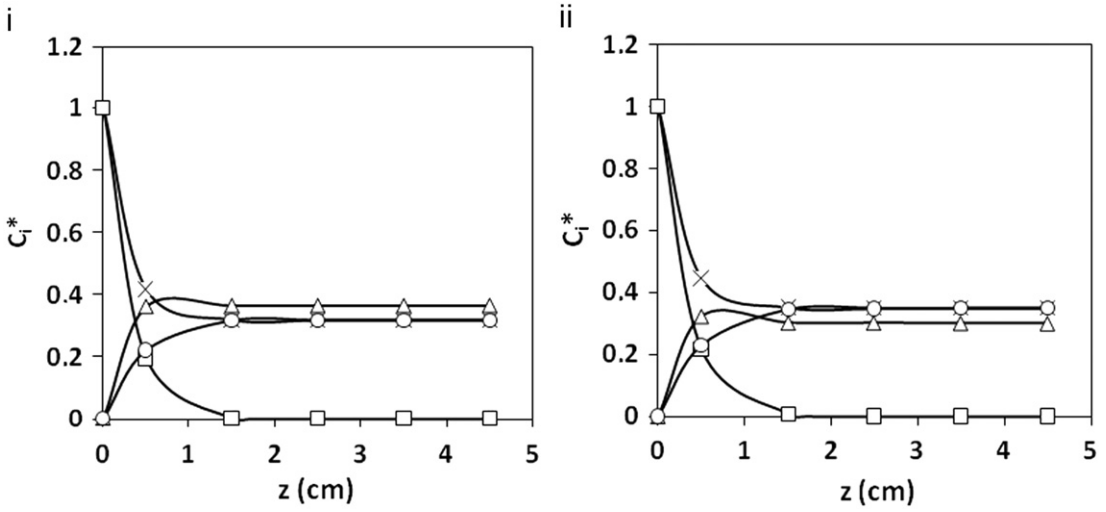

Fig. 5. Normalized concentrations C_i^* (symbols: *x*—C_A^*; □—C_B^*; △—C_P^* and ○—C_S^*) vs. tube length (i) without mixing at sub-grid scale ($C_\Phi=0$) (ii) with complete mixing at sub-grid scale ($C_\Phi=10^4$). Reaction rate coefficients $k_1=k_2=200\ m^3\ mol^{-1}\ s^{-1}$, feed ratio $\gamma=1$ and Rt=0.8. The calculated concentrations are obtained from Eqs. (12) and (14).

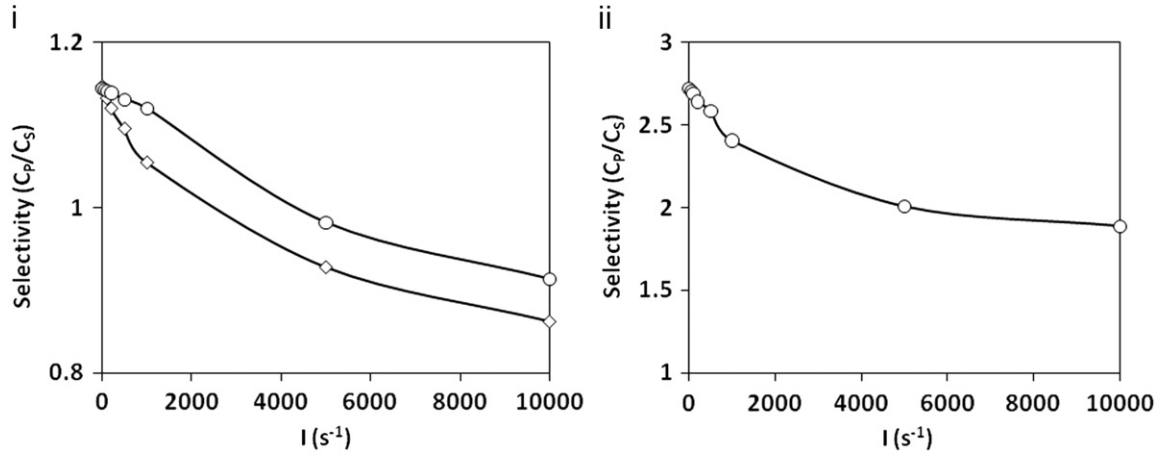

Fig. 6. Selectivity vs. mixing intensity for fixed feed ratio $\gamma=1$, Rt=0.8 and different reaction rate coefficients: (i) $k_1=k_2=10^4\ m^3\ mol^{-1}\ s^{-1}$ (symbol: ○) and $k_1=k_2=200\ m^3\ mol^{-1}\ s^{-1}$ (symbol: ◇) and (ii) $k_1=600$ and $k_2=200\ m^3\ mol^{-1}\ s^{-1}$. The calculated selectivity is obtained from Eqs. (12) and (14).

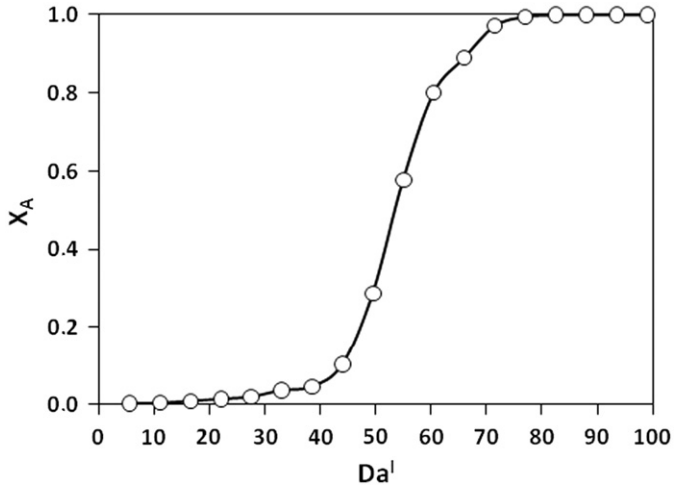

Fig. 7. Conversion of A vs. Da^I number, for $\beta=1$ and $\gamma=0.02$. The calculated conversions are obtained from Eqs. (12) and (14).

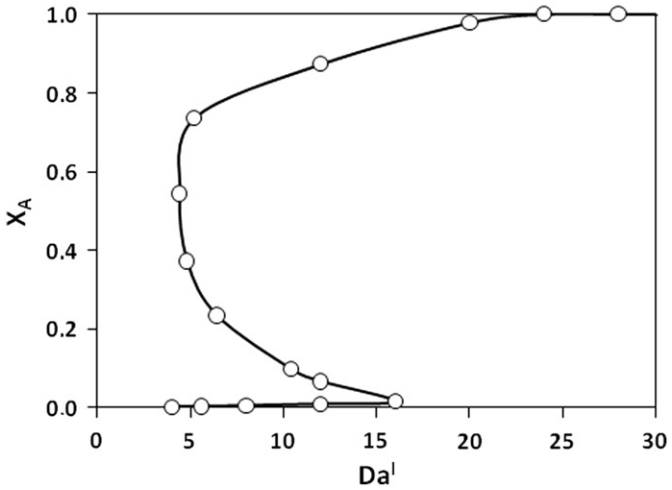

Fig. 8. Conversion of A vs. Da^I number, for $\beta=20$ and $\gamma=0.02$. The calculated conversions are obtained from Eqs. (12) and (14).

In the present work, results are obtained for different values of Péclet (Pe) and Damköhler (Da^I) numbers.

The Da^I number in the reactor is defined by the ratio of the time scale of convection and of reaction.

$$Da^I = LR(C_r)/(u_z C_r) \tag{26}$$

The Pe number in the reactor is defined by the ratio of the convective and diffusive flows of the reaction components.

$$Pe = u_z L/D_{AB} = u_z L\tau_u/(L_e^2 C_\Phi) \tag{27}$$

Note that Pe can be considered as the IEM model parameter, i.e. C_Φ value, because for a given flow field it is solely dependent on C_Φ.

The ratio of both these numbers is referred to as

$$\beta = Da^I/Pe \tag{28}$$

Furthermore, the integral length scale is determined as

$$L_e \approx k^{3/2}/\varepsilon \tag{29}$$

where k is the turbulent kinetic energy and ε is the turbulent dissipation energy.

Note that the correlation between β and C_Φ is determined by Eqs. (26) and (27) (rising C_Φ results in rising β for a specified Da^I).

Using the FV–PDF solution method, time dependent solutions for the problem are obtained. There is only one solution possible when performing time progressing simulations based on the initial guesses for the reaction components. The presented results are statistically steady state solutions for a given Da^I and Pe number.

The effect of the mixing on the conversion is shown in Figs. 7 and 8. From Fig. 7, it is concluded that only one conversion is calculated if the ratio of the Da^I and e number (β) equals 1, over the entire range of Da^I numbers for a given low feed ratio γ. On the other hand, for the same low feed ratio γ but with increasing β, i.e. with an increasing value of the Da^I number as compared to the Pe number, multiple conversions are calculated as seen in Fig. 8.

As seen in this bifurcation diagram Fig. 8, multiple solutions for the conversion are possible for a high ratio of the Da^I and Pe number ($\beta=20$). However, these multiple solutions are only calculated in the range of $5 \le Da^I \le 16$ for the given low feed ratio γ of 0.02. These results are in good agreement with the work of Gupta and Chakraborty (2009).

In Fig. 9, the conversion profiles for different C_Φ values of 0, 0.5 and 1, corresponding to low β ($\beta<1$) for the given low feed ratio γ of 0.02 are presented. For this range of C_Φ values, no multiple solutions are observed. On the other hand, for high values of C_Φ

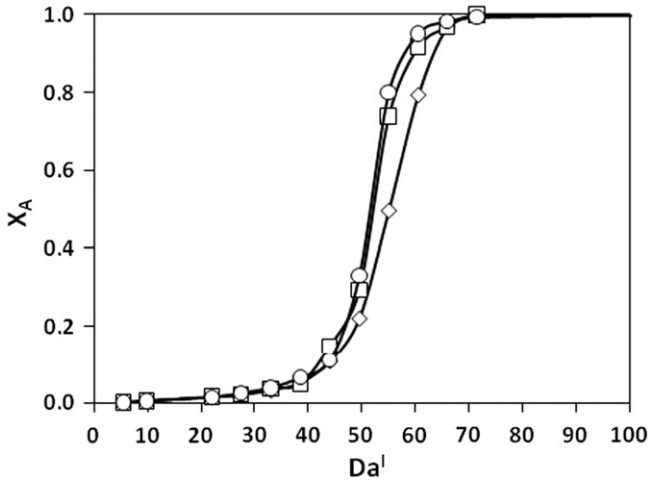

Fig. 9. Conversion of A vs. Da^I number, for different mechanical-to-scalar time-scale ratio, $C_\Phi=0$ (◇), $C_\Phi=0.5$ (□) and $C_\Phi=1$ (○) with constant feed ratio $\gamma=0.02$. The calculated conversions are obtained from Eqs. (12) and (14).

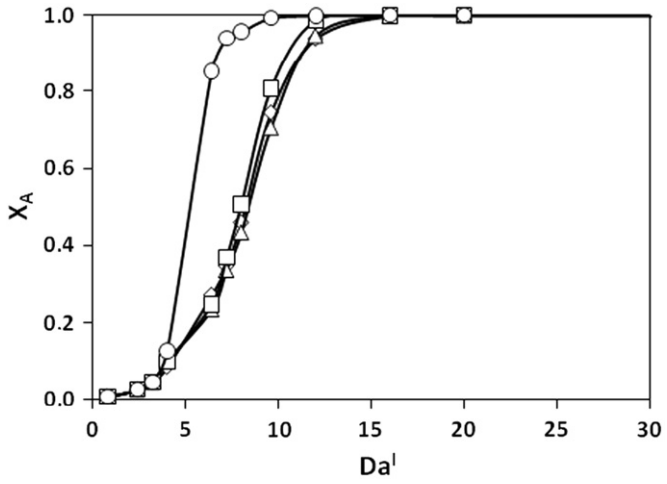

Fig. 10. Conversion of A vs. Da^I number, for different mechanical-to-scalar time-scale ratio, $C_\Phi=0$ (◇), $C_\Phi=1$ (△), $C_\Phi=10$ (□) and $C_\Phi=100$ (○) with constant feed ratio $\gamma=0.1$. The calculated conversions are obtained from Eqs. (12) and (14).

(i.e. high β), multiple solutions are observed (not shown) for the same feed ratio γ of 0.02.

When comparing Figs. 8 and 10, it is found that when increasing the feed ratio (γ) from 0.02 to 0.1, only one steady state solution is obtained over the entire range of the Da^I number as discussed in Gupta and Chakraborty (2009). This is due to the fact that the higher input concentration of the component B results in a very fast reaction (Eq. (24)) with an almost instantaneous consumption of the component A. Furthermore, a single steady-state solution is also observed over the entire range of β, with varying mechanical-to-scalar time-scale ratio, i.e. for every IEM model parameter value (Pe), and a high input concentration of *B*, as seen in Fig. 10.

As seen in Fig. 9, considerable differences in the conversions are found in the Da^I number range 40–60, even for small variations of the mechanical-to-scalar time-scale ratio C_Φ, when the input concentration of component B is low ($\gamma=0.02$).

From Fig. 10, it is concluded that for a specified conversion of *A*, the corresponding Da^I number range is very low as compared to Fig. 9, for the same range of C_Φ values (i.e. 0–1). This low Da^I number range in Fig. 10 is due to the condition of high input of B ($\gamma=0.1$). The latter increases the rate of reaction as compared to reduced feed of B ($\gamma=0.02$) in Fig. 9.

Furthermore, when the mechanical-to-scalar time-scale ratio C_Φ changes from 0 to 100, as seen in Fig. 10, the calculated conversion for a given Da^I number rises more than considerably, however, without any multiplicity of solution, as was calculated in Fig. 8 for a lower feed of B ($\gamma=0.02$).

Finally, as seen in Fig. 10, the simulation results for values of C_Φ from 0 to 10 differ slightly, implying that the effect of mixing is similar in between both values of C_Φ, i.e. a low degree of mixing observed. For a C_Φ value of 100, corresponding to a high degree of mixing, the conversion of *A* rises much faster.

- With increasing IEM parameter C_Φ, i.e. decreasing Pe number referring to increasing degree of mixedness, the conversion of component A in the autocatalytic reaction (Eq. (24)) increases.
- With increasing reaction rate, i.e. increasing Da^I number, the conversion of component A in the autocatalytic reaction increases for all initial feed ratios (γ).
- For an initial feed ratio of $\gamma=0.02$, multiple solutions can be found in a limited range of Da^I numbers as also shown by Gupta and Chakraborty (2009).

6. Conclusions

A hybrid FV/PDF solution algorithm to solve the flow and the species continuity equations, is applied to investigate the effect of micromixing, feed ratio γ (C_{Bo}/C_{Ao}) and reaction rate coefficients k_i on series–parallel and autocatalytic turbulent reactive single-phase gas flow in an isothermal tubular reactor. In a series–parallel reaction (A+B→P; P+B→S), the calculated selectivity of the desired product 'P' increases with the reaction rate coefficient of its formation reaction. On the other hand, the calculated selectivity of the desired product 'P' drops with increasing micromixing rate for a given reaction rate coefficient. In an autocatalytic reaction (A+2B→3B), single or multiple solutions are simulated when varying the feed ratio from 0.1 to 0.02. For an initial feed ratio of 0.02, multiple solutions are simulated for a limited range of Da^I numbers. With increasing reaction rate and micromixing rate, the conversion of component 'A' in the autocatalytic reaction increases for all initial feed ratios. Numerically, the presented hybrid solution algorithm is validated by solving the Reynolds-averaged species continuity equations model using the FV technique. A good agreement is found between the results obtained for infinite-rate mixing conditions using both approaches.

Nomenclature

C	Concentration (mol m^{-3})
C_Φ	Mechanical-to-scalar time-scale ratio (-)
D	Molecular diffusivity ($m^2\ s^{-1}$)
Da^I	Damköhler number ($LR(C_r)/(u_z C_r)$) (-)
f_ϕ	Composition probability density function
g	Acceleration due to gravity ($m\ s^{-2}$)
I	Mixing intensity ($1/\tau_\varphi$) (s^{-1})
k	Turbulent kinetic energy for gas phase ($m^2\ s^{-2}$)
k	Reaction rate constant ($m^3\ mol^{-1}\ s^{-1}/m^6\ mol^{-2}\ s^{-1}$)
L	Length of the reactor (m)
L_e	Integral length scale (m)
m	Mass of notional particle (kg)
N	Number of notional particles (-)
N_{TA}	Number of time-averaged iterations (-)
Pe	Péclet number ($u_z L\tau_u/(L_e^2 C_\Phi)$) (-)
R	Reaction source term (mol $m^{-3}\ s^{-1}$)

Rt	Time ratio of t_{CSR} to t_{MMR} (-)
s	Shear stresses (kg m^{-1} s^{-2})
Sc	Schmidt number ($\mu/(\rho D)$) (-)
t	Time (s)
$\mathbf{u}$	Interstitial gas velocity vector (m s^{-1})
$\mathbf{y}$, $\mathbf{Y}$	Position vector (m)
X	Mole conversion (-)
d$\mathbf{W}$	Wiener-diffusion (s$^{-1/2}$)
z	Axial length (cm)
$< >$	Ensemble-averaged value

Greek notations

$\boldsymbol{\varphi}$	Composition vector (mol m^{-3})
ϕ_α	Composition variable (mol m^{-3})
ρ	Density (kg m^{-3})
μ	Viscosity of the gas (kg m^{-1} s^{-1})
γ	Feed ratio (-)
β	Ratio of Da^I–Pe (-)
ε	Turbulent dissipation energy for gas phase (m^2 s^{-3})
τ_Φ, τ_u	Micromixing and integral time scale (s)
$\boldsymbol{\psi}$	Composition space vector (mol m^{-3})
ψ_α	Composition variable (mol m^{-3})
$\boldsymbol{\Gamma}$	Turbulent diffusivity (m^2 s^{-1})
$\boldsymbol{\xi}$	Standardized joint normal random vector (-)
σ_k, σ_ε	Constants in the gas turbulence model of values: 1.0, 1.3
$C_{1\varepsilon}$, $C_{2\varepsilon}$	Constants in the gas turbulence model of values:
C_μ	1.44, 1.92 and 0.09

Subscripts

A	Component A
B	Component B
CSR	Complete segregation reactor
i	Component i
l	Grid cell number
MMR	Maximum mixedness reactor
o	Initial condition
P	Component P
r	Reference
S	Component S
sim	Simulation
TA	Time average
α	Scalar component

Superscripts

i	Iteration number
n	Notional particle
t	Turbulent
-	Time-averaged value
$*$	Normalized value

References

Apte, S.V., Mahesh, K., Moin, P., Oefelein, J.C., 2003. Large-Eddy simulation of swirling particle-laden flows in a coaxial-jet combustor. International Journal of Multiphase Flow 29, 1311–1331.

Balakotaiah, V., Chakraborty, S., 2003. Averaging theory and low-dimensional models for chemical reactors and reacting flows. Chemical Engineering Science 58, 4769–4786.

Bird, R.B., Stewart, W.E., Lightfoot, E.N., 2002. Transport Phenomena second edition John Wiley & Sons.

Bourne, J.R., Toor, H.L., 1977. Simple criteria for mixing effect in complex reactions. AIChE Journal 23, 602–604.

Bourne, J.R., Kozicki, F., Rys, P., 1981. Mixing and fast chemical reactions—i. Test reactions to determine segregation. Chemical Engineering Science 36, 1643–1648.

Brodkey, R.S., Lewalle, J., 1985. Reactor selectivity based on first-order closures of the turbulent concentration equations. AIChE Journal 31, 111–118.

Cassiani, M., Franzese, P., Giostra, U., 2005. A PDF micromixing model of dispersion for atmospheric flow. Part I: development of the model, application to homogeneous turbulence and to neutral boundary layer. Atmospheric Environment 39, 1457–1469.

Chakraborty, S., Balakotaiah, V., 2002. Low-dimensional models for describing mixing effects in laminar flow tubular reactors. Chemical Engineering Science 57, 2545–2564.

Chakraborty, S., Balakotaiah, V., 2003. A novel approach for describing mixing effects in homogeneous reactors. Chemical Engineering Science 58, 1053–1061.

Das, A.K., De Wilde, J., Heynderickx, G.J., Marin, G.B., Vierendeels, J., Dick, E., 2004. CFD simulation of dilute phase gas–solid riser reactors: part I—a new solution method and flow model validation. Chemical Engineering Science 59, 167–186.

De Wilde, J., Marin, G.B., Heynderickx, G.J., 2003. The effects of abrupt T-outlets in a riser: 3D simulation using the kinetic theory of granular flow. Chemical Engineering Science 58 (3–6), 877–885.

Fox, R.O., 2003. Computational Models for Turbulent Reacting Flows first edition Cambridge University Press.

Gupta, A., Chakraborty, S., 2009. Linear stability analysis of high and low-dimensional models for describing mixing-limited pattern formation in homogeneous autocatalytic reactors. Chemical Engineering Journal 145, 399–411.

Hebb, T.G., Brodkey, R.S., 1990. Turbulent mixing with multiple second order chemical reactions. AIChE Journal 36, 1457–1470.

Kolhapure, N.H., Fox, R.O., Daiss, A., Maehling, F.O., 2005. PDF simulation of ethylene decomposition in tubular LDPE reactors. AIChE Journal 51, 585–606.

Li, K.T., Toor, H.L., 1986. Turbulent reactive mixing with a series–parallel reaction: effect of mixing on yield. AIChE Journal 32 (8), 1312–1320.

Mao, K.W., Toor, H.L., 1970. A diffusion model for reactions with turbulent mixing. AIChE Journal 16, 49–52.

Mehta, R.V., Tarbell, J.M., 1987. An experimental study on the effect of turbulent mixing on the selectivity of competing reactions. AIChE Journal 33 (7), 1089–1101.

Missen, R.W., Mims, C.A., Saville, B.A., 1999. Introduction to Chemical Reaction Engineering and Kinetics. John Wiley & Sons.

Pope, S.B., 1985. PDF methods for turbulent reactive flows. Progressive Energy Combustion Science 11, 119–192.

Pushpavanam, S., 2004. Mathematical Methods in Chemical Engineering. Prentice Hall of India.

Raman, V., Fox, R.O., Harvey, A.D., 2004. Hybrid finite-volume/transport PDF simulations of a partially premixed methane–air flame. Combustion and Flame 136, 327–350.

Sadarjoen, A., Walsum, T.V., Hin, A.J.S., Post, F.H., 1997. In: Nielson, G., Hagen, H., Müller, H. (Eds.), Particle Tracing Algorithms for 3D Curvilinear Grids, Scientific Visualization: Overviews, Methodologies, and Techniques. IEEE CS Press, pp. 311–335.

Subramaniam, S., Haworth, D.C., 2000. A probability density function method for turbulent mixing and combustion on three-dimensional unstructured deforming meshes. Journal of Engine Research 1, 171–190.

Toor, H.L., 1969. Turbulent mixing of two species with and without chemical reactions. Industrial and Engineering Chemistry, Fundamentals 8, 655–659.

Tsai, K., Fox, R.O., 1996. Modeling the scalar dissipation rate for a turbulent series - parallel reaction. Chemical Engineering Science 51, 1929–1938.

Vassilatos, G., Toor, H.L., 1965. Second-order chemical reactions in a nonhomogeneous turbulent field. AIChE Journal 11, 666–673.

Vegendla, S.N.P., Heynderickx, G.J., Marin, G.B., 2009. Probability density function simulation of turbulent reactive gas–solid flow in a riser. Chemical Engineering and Technology 32 (3), 492–500.

Villermaux, J., 1986. Micromixing phenomena in stirred reactors. Encyclopedia of Fluid Mechanics, vol. 2. Guff Publishing Company, Houston, pp. 707–771.

Vrieling, A.J., Nieuwstadt, F.T.M., 2003. Numerical simulations of competitive–consecutive reactions in turbulent channel flow. TU Delft, Ph.D. thesis.

Yablonsky, G.S., Constales, D., Marin, G.B., 2009. A new approach to diagnostics of ideal and non-ideal flow patterns: I. the concept of reactive-mixing index (REMI) analysis. Chemical Engineering Science 64 (23), 4875–4883.